Generation of large indium clusters by sputtering

C. Staudt and A. Wucher
Institute of Experimental Physics, University of Essen, 45117 Essen, Germany
(Received 18 March 2002; published 26 August 2002)

We have investigated the yields of neutral and charged In_n clusters sputtered from a pure indium surface under bombardment with 15-keV Xe^+ ions. It is shown that large neutral clusters containing up to 200 atoms can be detected. If the measured signals are corrected for size-dependent detection efficiency, an inverse power-law yield distribution according to $n^{-\delta}$ is found which exhibits two decay exponents of -3.9 for small ($n \leqslant 20$) and -2.1 for large ($20 \leqslant n \leqslant 100$) clusters. This finding closes the gap between published mass spectrometric and electron microscopy data on the size distributions of sputtered clusters. It also indicates that the generation of large clusters in sputtering is governed by hydrodynamical or even thermodynamical mechanisms rather than the fast collisional processes leading to the emission of small clusters.

DOI: 10.1103/PhysRevB.66.075419 PACS number(s): 79.20.Rf, 61.46.+w, 36.40.−c

I. INTRODUCTION

If a solid is bombarded with keV ions, particles are released from the surface due to mostly elastic collisions, a process which is generally termed sputtering. It is well known that the flux of particles ejected from the surface this way may contain agglomerates of several atoms (besides atomic species).[1] In particular, much interest has been devoted to the detection of large clusters containing 100 or more atoms, since the basic mechanisms leading to the formation and emission of such large entities in sputtering represent one of the fundamental open questions in the field. Most of the earlier work has been performed using the mass spectrometry of secondary ions—i.e., those particles that leave the surface in an electrically charged state. Using this technique, Katakuse *et al.*[2] have been able to detect sputtered ionized metal clusters containing up to more than 200 atoms. The physical mechanisms leading to the ionization of a sputtered cluster, however, are not well understood. It is therefore highly questionable as to what extent the flux of secondary ions is actually representative of the total sputtered flux of the respective species. In fact, it has been demonstrated that the ionization probability of sputtered clusters may significantly depend on the cluster size.[3] In order to arrive at quantitative conclusions regarding the contribution of clusters to the total sputtered flux, it is therefore mandatory to complement the secondary-ion data by investigating those species which leave the surface in a neutral-charge state. In order to render them accessible to mass spectral analysis, these particles have to be post-ionized subsequent to their emission from the surface. Moreover, the post-ionization technique employed needs to be sufficiently soft to avoid significant fragmentation of the sputtered species. While earlier post-ionization schemes involving electron impact ionization restricted the size of detectable neutral clusters to about four atoms,[4] laser-based photoionization methods have recently evolved which allow the detection of much larger clusters. A very promising technique in that respect is ''single-photon ionization'' (SPI), where photoionization is achieved by non-resonant absorption of only one photon from an intense pulsed laser beam, thus avoiding ultrafast fragmentation losses from excited intermediate states which often accompany multiphoton ionization schemes of molecular species. In order to overcome the ionization potential, the use of SPI requires use of UV or even VUV radiation which must be produced with sufficient intensity to render the photoionization process efficient. Such photon fluxes can, for instance, be generated by excimer or F_2 gas lasers emitting at wavelengths of 248, 193, or 157 nm, respectively. Using that technique in combination with time-of-flight mass spectrometry, sputtered neutral metal clusters containing up to about 50 atoms have been detected. Moreover, it has been demonstrated that the available photon flux density produced by such a laser often even suffices to drive the post-ionization process into saturation, a possibility which eliminates the need of knowledge about photoionization cross sections in order to arrive at a quantitative characterization of the flux of sputtered neutral particles.[5,6]

As a consequence, yields of sputtered clusters have been determined for various metallic target materials bombarded with different projectile ions of varying kinetic energies.[5–20] In practically all cases investigated so far, a monotonically decreasing yield distribution is observed which closely follows an inverse power-law decay with increasing cluster size, the exponent of which is found to be correlated with the total sputtering yield. More specifically, the contribution of larger clusters is always enhanced if the sputtering conditions are changed such as to lead to a higher sputtering yield and vice versa. So far, no theoretical model of cluster formation in sputtering has been published that describes this phenomenon. The only model calculations predicting power-law cluster yield distributions are based on either a shock-wave[21] or a thermodynamic equilibrium[22] description of the cluster formation process. In both cases, the predicted decay exponent is fixed at values around -2, whereas the exponents measured in the mass spectrometric experiments vary in a range from -9 to about -4. Most recently, Rehn *et al.* have employed a very much different electron microscopic technique in order to determine the size distribution of very large clusters ($n \geqslant 500$) sputtered from a gold surface by high-energy rare gas ion impacts.[23] Also in this work, an inverse power-law distribution is observed with, however, a decay exponent around -2, which seems to be independent of the sputtering yield. This finding suggests that the shock-wave or

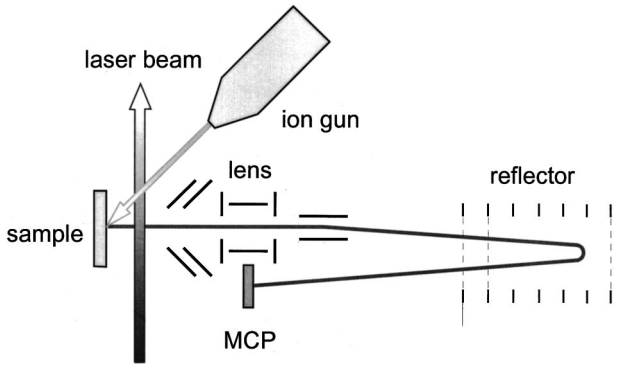

FIG. 1. Schematic setup used for time-of-flight mass spectrometric detection of sputtered neutral and ionized atoms and clusters.

thermodynamic equilibrium cluster formation model might work to describe the yield distribution of very large clusters containing several hundred up to several thousand atoms. In order to close the gap between the existing mass spectrometric and electron microscopy data, it is therefore very important to extend the mass spectrometric experiment to larger cluster sizes. In the present paper, we describe corresponding results obtained for homonuclear In_n clusters sputtered from a pure indium surface. In the range $n \leqslant 32$, this system has already been investigated by Ma *et al.*,[9] who bombarded an indium surface with normally incident 3.75-keV Ar^+ ions and found power-law yield distributions with exponents of -5.6 and -4.1 for neutral and ionic In_n clusters, respectively. Using higher-energy projectiles, we will show that clusters containing up to $n=200$ are detectable. For these cluster sizes, the detection probability at the particle detector used for registration of the cluster ions becomes increasingly important. In an attempt to correct the measured data for the cluster size dependence of the detection probability, we vary the impact energy of the ions onto the detector and compare the resulting data with published model descriptions of secondary-electron multiplier detection efficiencies. The results will demonstrate that (i) the detection probability correction is very important and (ii) the shock-wave or thermodynamic formation models may indeed be valid for large sputtered clusters.

II. EXPERIMENT

The experimental setup used for mass spectrometric detection of sputtered neutral and ionized atoms and clusters is sketched in Fig. 1. The setup and the procedures employed to obtain mass and kinetic energy spectra of sputtered neutral and charged particles have been described in much detail elsewhere[6,24] and will therefore only be briefly touched upon here. The investigated sample surface is bombarded with projectile ions generated by a commercial plasma gas ion source (Atomica microfocus) delivering a Xe^+ ion beam of 15 keV and 500 nA into a spot size of about 60 μm diameter. The primary ions impinge onto the surface under 45° with respect to the surface normal. In these experiments, the projectile ion source was operated in a pulsed mode with pulse lengths ranging from 100 ns to 10 μs. Neutral particles sputtered from the surface are post-ionized by single-photon absorption from an intense, pulsed UV laser beam operated at a wavelength of 193 nm, pulse energies up to 150 mJ, and a pulse duration of about 20 ns. In connection with the applied focal conditions (beam cross-sectional area of about 1 mm^2) and the limited transmission of the optical components, this results in peak power densities in the ionization volume, i.e., the volume where the ionization laser interacts with the sputtered neutral species, up to about 3×10^7 W/cm^2, which could be varied over several orders of magnitude by a set of two dielectric attenuators. The ions produced by the photoabsorption process are swept into a reflectron-type time-of-flight (TOF) mass spectrometer by means of a pulsed electric field that is switched on about 20 ns after the ionizing laser pulse. Secondary ions leaving the bombarded surface are detected by simply switching off the ionization laser and leaving the remainder of the experiment unchanged. As explained in detail elsewhere,[24] this operation mode ensures that secondary ions and neutrals are detected under exactly the same experimental conditions with respect to the sampled solid angle, the sampled emission velocity interval, and the mass spectrometer detection efficiency. Assuming similar emission angle and velocity distributions of secondary ions and neutrals, the secondary ion formation probabilities can therefore be estimated by simply comparing the respective signals of ions and neutrals, provided the post-ionization efficiency for the neutral species is known. As will be illustrated below, the available laser intensity is high enough to drive the photoionization process into saturation, thereby eliminating the *a priori* unknown photoionization cross section.

During the measurements determining the total yield of sputtered atoms and clusters, a relatively long projectile ion pulse of several μs duration was chosen. More specifically, it was ensured that the measured signals did not increase with increasing pulse length, thus indicating that particles of all relevant emission velocities are present in the ionization volume and interact with the ionizing laser. In order to determine the emission velocity distributions of sputtered neutral particles, on the other hand, the laser was focused to a cross section of about 100 μm$\times$500 μm [full width at half maximum (FWHM)] with the short dimension being normal to the surface. Moreover, the laser was attenuated to a peak power density of about 1 MW/cm^2 and backed away from the surface to a distance of 2.2 mm, the primary ion pulse width was reduced to 100 ns, and a controlled time delay between the projectile ion and the ionizing laser pulse was introduced. This operation mode selects the emission velocity of the detected neutral particles via their flight time between the surface and the ionization volume with a resolution of $\Delta\nu/\nu \approx 4.5\times10^{-2}\{1+\nu\ (\mathrm{km/s})\}$. The velocity spectrum of sputtered neutral atoms and clusters is then determined by following the respective photoion signal as a function of the delay time.

The mass selected ions were detected by means of a Chevron stack of two microchannel plates (MCP's). During registration of neutral atoms and small clusters, a flight time peak is composed of many ions, and therefore an analog detection scheme was employed in which the charge pro-

duced by the MCP was directly digitized by means of a fast transient recorder. In order to avoid detector saturation, the gain voltage across the MCP was reduced such as to ensure that the maximum recorded signal did not exceed a height of about 100 mV (at 50 Ω termination). For larger clusters, the signals of abundant species were blanked from reaching the detector, and a pulse counting mode was employed where the MCP was operated at maximum gain and its output was coupled into a discriminator. In this mode, each output pulse exceeding a height of about 1 mV was converted into a standard transistor-transistor logic (TTL) pulse of 5 V height and 20 ns width: the resulting pulse spectrum was again recorded using the transient digitizer. Time-of-flight spectra were in this mode achieved by averaging the recorded pulse spectrum over many instrument cycles (primary ion pulses and laser shots). In order to investigate the influence of the cluster-size-dependent detection probability, different voltages were applied to the front electrode of the MCP while keeping the gain voltage constant. This way, the kinetic impact energy of the ions onto the MCP surface was varied in a range between 3.7 and 6.2 keV.

III. RESULTS AND DISCUSSION

The major goal of the present work is to determine the relative yields—i.e., the partial sputtering yields normalized to that of emitted monomers, of large In_n clusters emitted from an ion-bombarded indium surface. In doing so, we first show the TOF mass spectrum measured for sputtered neutral particles in order to demonstrate the mass-resolved detection of clusters up to a fairly large size. As a second step, we investigate the dependence of the measured neutral signals on the intensity of the ionizing laser. From the results, we will show that saturated post-ionization conditions can be achieved. By comparing the saturated neutral signal with the signal of the respective secondary ions, we then determine the secondary-ion formation probability of the sputtered clusters in order to judge how closely the neutral yields represent the true partial sputtering yields. Since the TOF experiment performed here detects the *number density* of sputtered neutral or charged particles in the ionization volume rather than their *flux*, an appropriate correction must be applied to the measured signals which, in turn, involves the velocity distribution of the detected species. In general, sputtered particles are emitted from the surface with a relatively broad velocity distribution, which may in principle be different for every emitted species. We therefore measure the emission velocity distribution as a function of the cluster size and use these data to perform the density-flux correction individually for each cluster size. The resulting corrected signals represent the partial yields of sputtered clusters superimposed by the detection probability of the MCP ion detector. The latter quantity may in principle strongly depend on the size of the detected cluster. In the last step, we therefore try to tackle the question of the cluster-size-dependent detection probability. The resulting yield distributions of sputtered indium clusters are then compared with available literature data and discussed in terms of theoretical model descriptions of cluster formation in sputtering.

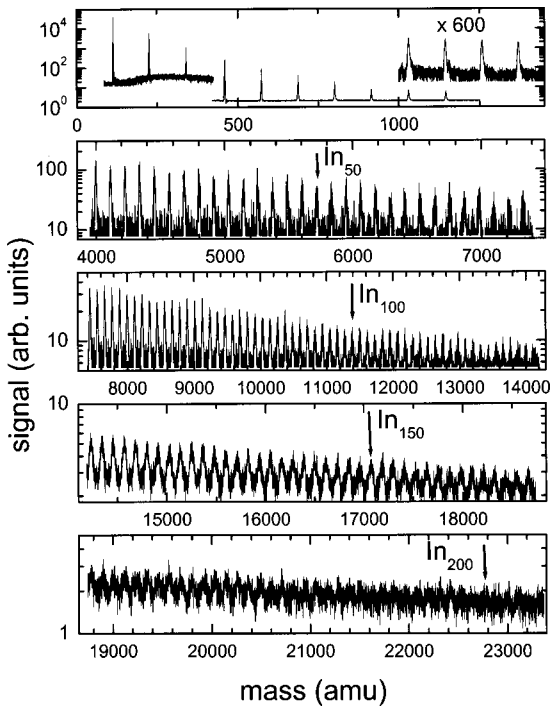

FIG. 2. TOF mass spectrum of neutral In atoms and In_n clusters sputtered from a pure indium surface under bombardment with 15-keV Xe^+ ions impinging under 45° with respect to the surface normal. The ionizing laser was operated at a wavelength of 193 nm and a power density of about 10^5 W cm^{-2}.

A. Mass spectra

Figure 2 shows a mass spectrum of neutral atoms and clusters that are sputtered from a clean polycrystalline indium foil. The spectrum was recorded under bombardment with 15-keV Xe^+ ions impinging under 45° using 193-nm UV radiation with a laser power density around 10^5 W/cm^2 for post-ionization. The mass spectrometer is operated at a resolution of about $m/\Delta m = 500$, which appears to be approximately constant across the whole spectrum. The lower two tracks in the first panel correspond to the analog detection mode, whereas the upper track as well as all data in the remaining panels were taken with the pulse counting mode. In order to achieve the displayed dynamic range of about 7 orders of magnitude, the spectrum has been averaged over a number of 10^4 instrument cycles (primary ion pulses and laser shots). It is seen that neutral indium clusters up to $n = 200$ atoms can be identified in the mass spectrum. For cluster sizes in this range, the mass peaks of neighboring clusters become indiscernible due to the limited mass resolution combined with the inherent width induced by the isotope distribution of indium (about 20 dalton at In_{200}).

It is of interest to note that particles of masses larger than 20 000 dalton can be identified in the spectrum. To our knowledge, these are the largest neutral clusters detected in a mass spectrometric sputtering experiment to date. From the results presented in Fig. 2, it is evident that the size range of *neutral* clusters formed in sputtering extends to comparably large values as that of *ionic* clusters that have been detected, for instance, by Katakuse *et al.*[2,25,26] Although this finding

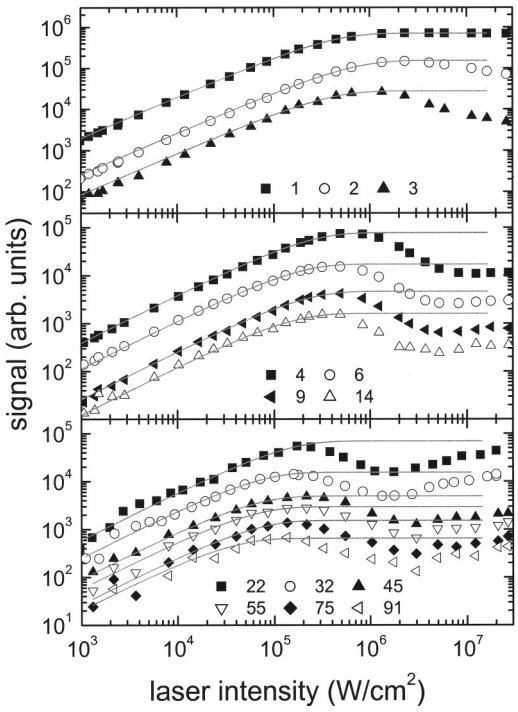

FIG. 3. Integrated signals of post-ionized sputtered neutral In_n particles vs peak power density of the ionizing laser.

was in principle expected, a mass spectrometric verification of the occurrence of sputtered neutral clusters containing more than 100 atoms has been lacking until now.

B. Post-ionization efficiency

In order to obtain quantitative information from mass spectra like those displayed in Fig. 2, it is important to get a feeling for the ionization efficiency achieved in the post-ionization process. If photoionization is employed in connection with sufficiently intense lasers, the available photon fluxes might even be sufficient to drive the post-ionization process into saturation. To demonstrate this effect also for the system studied here, Fig. 3 shows the dependence of the measured integrated mass peaks on the peak power density of the ionizing laser. The numeric values depicted on the abscissa have been calculated assuming a rectangular temporal laser pulse profile of 20 ns duration and a measured beam cross section of 1 mm^2 in the ionization volume. The absolute uncertainty introduced by these assumptions may amount to a factor of 2, but the relative values are free from this systematic error. First of all, it is seen that the photoionization efficiency observed for the indium atom perfectly agrees with the theoretically expected saturation behavior according to

$$S(P_L) = S_{\mathrm{sat}}\left[1 - \exp\left(-\sigma \frac{P_L}{h\nu}\Delta t\right)\right], \qquad (1)$$

with σ being the photoabsorption cross section, $h\nu$ being the photon energy, and Δt being the laser pulse duration, as seen by the respective least-squares fit, which is shown as a solid line. The observation of a true saturation plateau ensures that the laser beam profile has been matched to the sensitive volume of the mass spectrometer, and hence no expansion of the effective ionization volume occurs with increasing laser intensity. This fact is important for the interpretation of the dependences observed for clusters. From the saturation curves depicted in Fig. 3, it is seen that all cluster signals rise linearly with increasing laser intensity in the regime of low intensity, a finding which is expected from Eq. (1). At intensity values around or below 10^6 W/cm^2, all cluster curves flatten due to saturation of the single-photon ionization process. Since the saturation intensity apparently decreases, the value of the absorption cross section must increase with increasing cluster size, a finding which is in agreement with similar data observed for other metal clusters.[14] It should be noted that fragmentation processes competing to ionization following absorption of a single photon lead to the same shape of the saturation curve and are included in the cross section σ entering Eq. (1). The relative importance of such processes cannot be determined from the measured data and must therefore be regarded as an unknown quantity. If the laser intensity is increased further, the measured signal is found to turn over and decrease again. This behavior must be attributed to the onset of multiphoton fragmentation processes which require the simultaneous absorption of more than one photon and can therefore be assumed to play only a minor role at low laser intensities. In the limit of large laser intensity, the curves tend to level off and in some cases even increase again. At first sight, this behavior appears surprising. Considering losses due to fragmentation alone, the signal must of course always decrease with increasing laser intensity. The fact that the measured signal either remains constant or even increases must therefore be attributed to fragmentation of larger clusters starting to contribute to the signal of a given cluster size. With ever increasing laser intensity, the signal will be shifted towards smaller and smaller clusters, until in the limit of very high laser intensities all clusters are fragmented and only the atomic signal survives. A quantitative discussion of this phenomenon, however, requires precise knowledge of the various fragmentation channels and the associated cross sections which is not available at the present time.

By applying a least-squares fit of Eq. (1) to the measured data in the laser intensity range up to the observed signal maximum, saturation intensities as well as photoabsorption cross sections can be obtained for all cluster sizes. The resulting fit curves have been included in Fig. 3, and the corresponding values of the single-photon absorption cross section are depicted in Fig. 4. Again, we note that the evaluation leading to the assessment of the data assumes multiphoton fragmentation influences to be small at all laser intensities below the observed maxima and is therefore subject to some uncertainty. Interestingly, it is found that the apparent absorption cross section of indium atoms is larger than that of In_2 dimers. This behavior is different from that observed for other sputtered metals.[14] For clusters containing more than two atoms, the cross section increases with increasing cluster size and reaches a constant value of about 10^{-15} cm^2. The apparent structure at sizes of about 8, 17, and 38 atoms does not seem to be related to either magic shell closing numbers

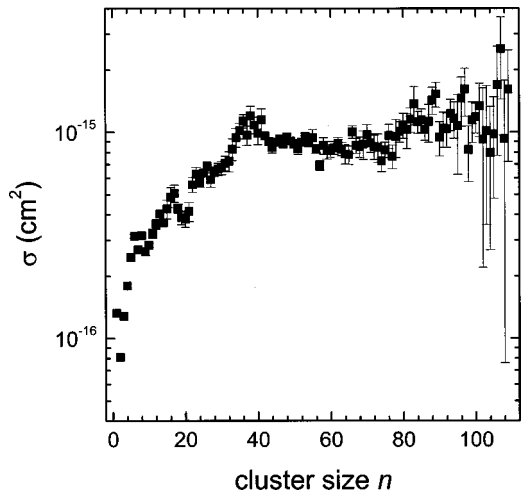

FIG. 4. Single-photon absorption cross section of sputtered neutral indium atoms and clusters at a wavelength of $\lambda = 193$ nm vs cluster size.

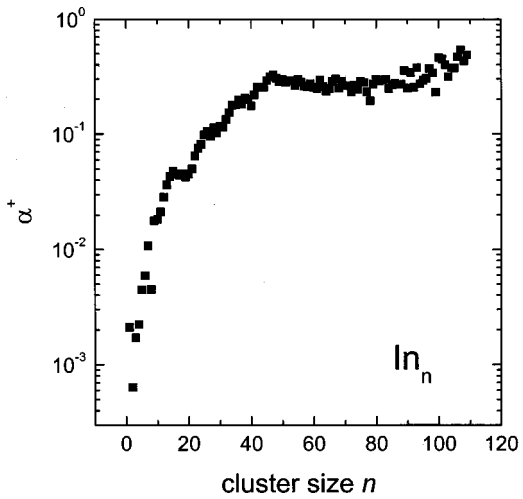

FIG. 5. Ionization probability of sputtered In atoms and In_n clusters for the formation of a singly charged positive secondary ion during sputtering vs cluster size *n*.

or similar structures in the measured ionization potentials of indium clusters.[27] From the solid lines, it is seen that in all cases the saturated signal evaluated from the fit practically coincides with the signal maximum itself, thus indicating that saturation is complete before multiphoton fragmentation starts to play an important role. We therefore regard the saturated signal as representative of the number density of the respective neutral cluster in the ionization volume. It should be stressed once again, however, that the unknown role of single photon fragmentation may lead to an underestimation of the true number densities which cannot be identified from laser power studies. The cluster yields that are derived from the saturated signal must therefore rigorously be interpreted as lower limits of the true yields.

C. Charge-state distribution

If the measured signal of a neutral cluster is to be interpreted in terms of its partial sputtering yield, it is important to ask about the fraction of sputtered clusters that are emitted as secondary ions—i.e., in an electrically charged state. For the specific case of clean metallic surfaces bombarded with rare gas ions, it is known that the yield of negatively charged atoms and clusters is negligibly small. In order to determine the fraction of positively charged clusters, the experiment was repeated with the ionization laser switched off, but under otherwise identical conditions. As described in detail elsewhere,[24] the secondary-ion formation probability of a sputtered species can then be determined from direct comparison of the secondary-ion signal with the respective neutral signal obtained under saturated post-ionization conditions. The results are displayed as a function of cluster size in Fig. 5. In agreement with similar data measured for other sputtered metal clusters,[3] the secondary-ion formation probability is found to increase with increasing cluster size and tends to level off at sizes above approximately 40 atoms at a value of several ten percent.

The saturation value observed in the limit of large cluster size is larger than that determined for Ag_n, but below those determined for Ta_n and Nb_n clusters. About the reason for this finding we can only speculate. It is conceivable that the ionization of a sputtered cluster involves thermionic emission of an electron—i.e., the conversion of internal vibrational energy originating from the sputter formation process into electronic excitation and ionization, after the cluster has left the surface. In this picture, the ionization probability will be determined by a balance between ionization potential and average internal energy imparted to the clusters in the course of the sputtering process. The latter, on the other hand, will be related to the bond strength between the cluster atoms. Tantalum and niobium clusters are known to exhibit binding energies per atom that are comparable to their ionization potential. In this case ionization will be highly probable [up to about 100% (Ref. 3)]. Silver clusters, on the other hand, possess ionization potentials that largely exceed their binding energy per atom, and therefore ionization seems to be less probable (about several percent[3]). The indium clusters studied here possess lower binding energy, but also lower ionization potential than silver clusters, and must therefore form an intermediate case.

The signal of multiply charged secondary ions can in principle be identified as intermediate peaks in the mass spectrum arising, for instance, from doubly charged clusters with an odd number of constituent atoms. In the present experiments, multiply charged secondary ions have not been detected. Using the values depicted in Fig. 5, the saturated signals of sputtered neutral atoms and clusters can therefore be corrected for the secondary-ion formation probability, thus resulting in yield data that are independent of the charge state of the emitted particles.

D. Velocity distribution

In the yield determination experiment, the ionization laser beam cross section is large enough that transport of neutral particles into and out of the ionization volume during the laser pulse is negligible for all velocities below approximately 50 km/s. Under these conditions, the laser post-

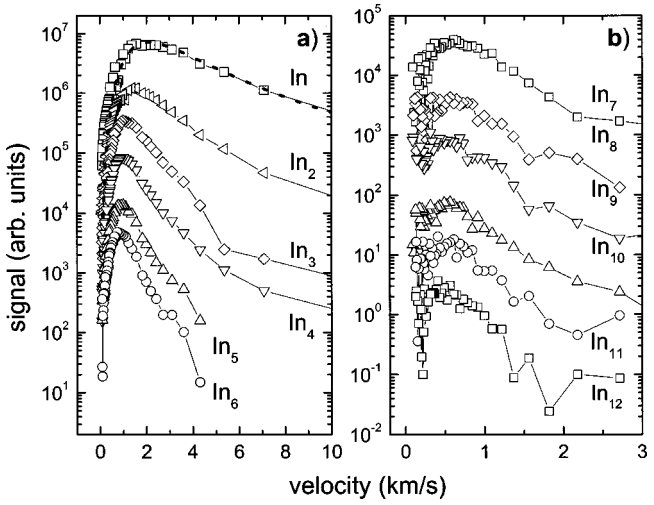

FIG. 6. Emission velocity distribution of neutral In atoms and In_n clusters sputtered from a pure indium surface under bombardment with 15-keV Xe^+ ions. The absolute scaling of the curves has been arbitrarily chosen to ensure clear visibility and is therefore not representative of the relative cluster yields.

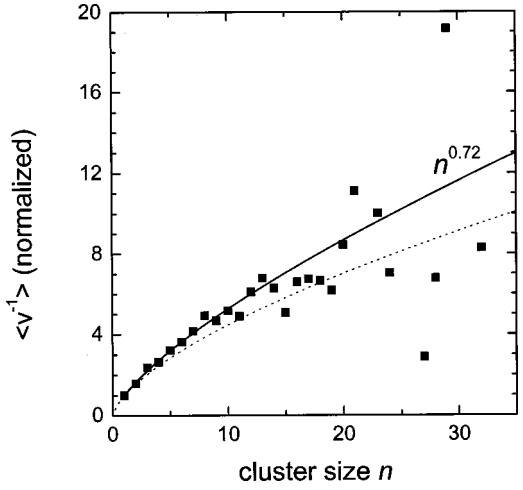

FIG. 7. Average inverse velocity of sputtered neutral indium clusters evaluated from the distributions of Fig. 6 and normalized to the respective value of indium atoms.

ionization experiment is sensitive to the number density of neutral particles that are present in the ionization volume. Sputtering yields, on the other hand, represent the flux of sputtered particles rather than their number density. In order to determine the yield distribution of sputtered clusters, the experimental data must therefore be converted from density to flux. For that purpose, the velocity of the post-ionized species must be known. Since sputtered particles emerge from the surface with a relatively broad velocity distribution, the measured signal must be divided by the average inverse velocity defined by

$$\langle \nu^{-1} \rangle = \int_0^\infty \nu^{-1} f(\nu) d\nu \tag{2}$$

for correction. In principle, the velocity distribution $f(\nu)$ can be different for each sputtered species and must therefore be determined as a function of the cluster size. Figure 6 shows corresponding data that have been measured using the method described in Sec. II. Note that the absolute scaling of the curves has been arbitrarily chosen to ensure good visibility and is therefore not representative of the relative cluster yields. Due to the fact that the laser beam was tightly focused during the velocity distribution experiments, care must be taken with regard to particle transport across the ionization volume during the laser pulse. In general, the Jacobian conversion between measured flight time distribution $S(t)$ and flux velocity distribution is given by[20]

$$f(\nu) \propto \frac{S(t)t}{\Delta r + \frac{r}{t}\Delta t}, \tag{3}$$

where Δr denotes the spatial extension of the ionization volume in the direction along the surface normal, r is the distance between ionization volume and surface, and Δt is the temporal duration of the laser pulse. As shown in Ref. 20, the second term in the denominator appears only if the post-ionization process is driven into saturation, a condition which in the present experiment is fulfilled for all detected species.

The data depicted in Fig. 6 appear to agree well with the results of a similar experiment that has been performed by Ma *et al.*[28] Moreover, the velocity distribution measured for In atoms can be compared to the prediction from linear cascade sputtering theory,[29]

$$f(\nu) \propto \frac{\nu^3}{(\nu^2 + \nu_b^2)^3}, \tag{4}$$

with ν_b being the velocity corresponding to the surface binding energy. Approximating the latter by the sublimation energy of indium (2.5 eV), one obtains the dotted curve in Fig. 6, which is in good agreement with the measured data. Evaluating the data depicted in Fig. 6 in terms of Eq. (2), we obtain average inverse velocity values which are displayed in a form normalized to that of the atoms in Fig. 7. Since the signal of clusters larger than In_{20} is too low to permit a meaningful determination of the velocity distribution, an extrapolation must be used in order to correct the yield measurements of larger clusters as well. For that purpose, we chose to perform a least-squares fit according to

$$\langle \nu^{-1} \rangle \propto n^b \tag{5}$$

to the data of Fig. 7. Due to the limited statistics of the velocity distributions of larger clusters, only values up to a cluster size of $n=13$ have been included. This yields a power of $b=0.72$: inclusion of all data depicted in Fig. 7 would reduce this value to 0.65. The resulting curves have been included in the figure as a solid and a dotted line, respectively. Equation (5) was then used to perform the flux-density correction by dividing the saturated signals by $n^{0.72}$.

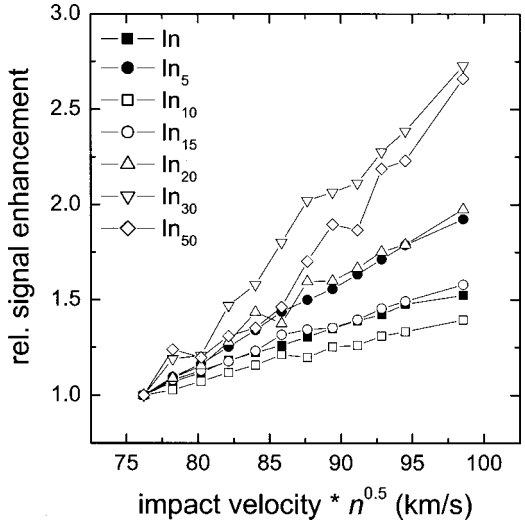

FIG. 8. Relative enhancement of detected ion signals vs ion impact velocity onto the detector. The data were normalized to the signal measured with an impact energy of 3.7 keV. In order to plot different cluster sizes n into one diagram, the velocity axis of each cluster was multiplied by $\sqrt{n}$. The solid symbols refer to analog detection, whereas the open symbols refer to the pulse counting mode (for definition see text).

E. Detection probability

The mass spectrum displayed in Fig. 2 reveals the detection of ions of masses up to about 22 000 dalton. At first sight, the mere registration of such heavy species with a simple Chevron stack MCP detector without strong post-acceleration seems to be surprising. Under our normal operation conditions applied during acquisition of Fig. 2, the particles impinge onto the detector with a kinetic energy of 3.7 keV: the impact velocity of the largest detected ions is therefore as low as 4.5 km/s, a value which is well in the range of typical straight line threshold [for definition see discussion of Eq. (7)] values measured for the velocity dependence of secondary electron yields.[30] The detection probability and its dependence on the size of the detected cluster ions must therefore be an important issue with respect to the quantitative determination of sputtered cluster yields. In order to investigate this problem, the kinetic impact energy onto the MCP detector was varied between 3.7 and 6.2 keV while keeping all other instrumental parameters including the gain voltage across the MCP constant. The resulting signal enhancement relative to that observed at 3.7 keV impact energy is depicted in Fig. 8. Since the impact *velocity* is often regarded as the essential parameter rather than the kinetic energy, the data have been plotted against velocity which—in order to be able to plot the data obtained for different cluster sizes n into one diagram—for each cluster was multiplied by $\sqrt{n}$. Moreover, the solid symbols refer to analog detection, whereas the open symbols refer to data taken in the pulse counting mode. First, it is seen that the relative enhancement increases with increasing cluster size. As expected, the influence of post-acceleration is therefore larger for heavier detected species. A more detailed discussion of the detection efficiency requires to distinguish between both detection modes.

1. Analog detection

In the analog mode, the observed MCP gain is determined by the ion-to-electron conversion efficiency upon impact of the ion at the front side of the detector and the secondary electron multiplication factor. Due to the fact that a detected flight time peak consists of many ions impinging simultaneously, the statistics of electron emission is not important and only average electron yields are needed in order to describe the observed gain. For the simplified case of a multistage secondary electron multiplier, one finds[31]

$$\text{gain} = \gamma_1 \cdot \gamma^p , \tag{6}$$

where γ_1 denotes the average ion-induced electron emission yield at the conversion electrode and γ denotes the secondary-electron emission yield at each of the p subsequent amplification dynodes. In principle, this expression can be generalized for an MCP detector as well, where p now is not a unique value but is a statistical average of the number of electron induced amplification events at the channel wall.[32] While the second term in Eq. (6) is solely governed by the gain voltage applied across the MCP, the influence of the ion impact energy is contained in the value of γ_1. Experimentally, it is often found that—at least in the limit of high velocities—kinetic ion-induced electron emission yields depend linearly on the ion impact velocity.[30] It is seen that this behavior is also found for In and In_5 in Fig. 8. In order to account for the deviations that are generally observed at low velocities, Gilmore and Seah[32] introduced a semiempirical formula

$$\gamma_1 = A\nu\left[1 - \left(\frac{1}{1+(\nu/\nu_0)^\kappa}\right)^{1/\kappa}\right], \tag{7}$$

with a scaling item A, the usual ''straight line threshold'' velocity ν_0, and a power κ as fitting parameters, and demonstrated that Eq. (7) provides excellent fits to various sets of available experimental data. Moreover, they assume that the yield for a polyatomic ion is simply the sum of the constituent yields, and therefore $A = an$ for the In_n clusters investigated here. Equation (7) then predicts a factor of $\sqrt{5}$ between the slopes of In and In_5 in Fig. 8, which is reasonably close to the observed slope ratio of about 1.7. For simplicity, we therefore assume the total MCP gain of all detected clusters in analog detection mode to be described by Eq. (7) with a common set of parameters a, ν_0, and κ, which still have to be determined.

2. Pulse counting

In the pulse counting mode, single-ion impact events are registered and, hence, the statistics of the electron emission process induced by the impinging ion becomes important. The theory describing the efficiency of secondary-electron multipliers in this mode is already well established.[31] Following the description by Seah,[31] we assume a Poisson probability distribution

$$P(m,\gamma) = \frac{\gamma^m}{m!} e^{-\gamma} \tag{8}$$

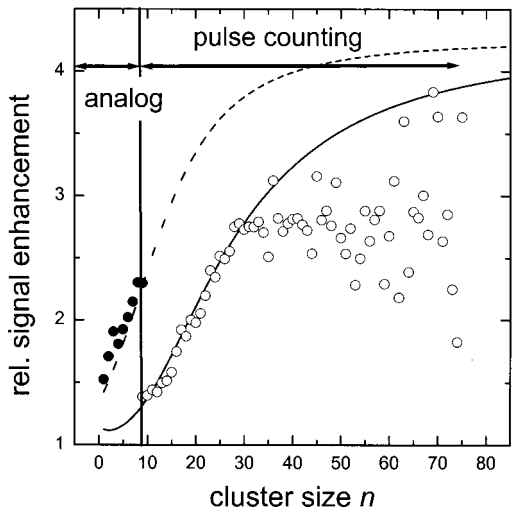

FIG. 9. Relative signal enhancement between detector impact energies of 3.7 and 6.2 keV, respectively, vs size of the detected cluster ions. The solid symbols refer to analog detection, whereas the open symbols refer to the pulse counting mode (for definition see text).

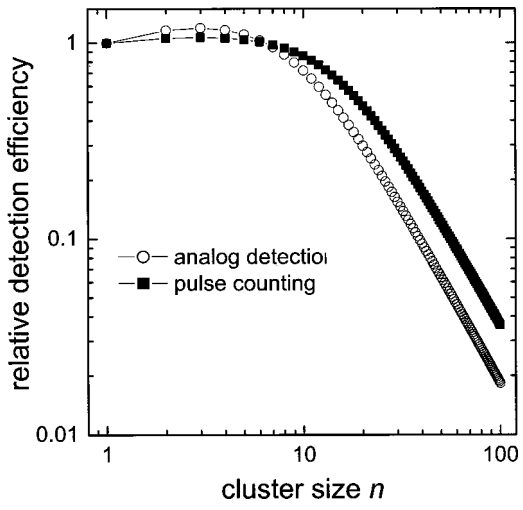

FIG. 10. Detection probability of In atoms and In_n clusters vs cluster size at "normal" operation of the MCP detector (impact energy 3.7 keV). The data have been calculated from Eqs. (6), (7), and (10) using the parameter set given in the test.

for the emission of m electrons in an event with average electron yield γ. The probability for detection of an ion impinging with energy E is then given by

$$D(E) = 1 - P_{01}(1 + \text{correction terms}), \tag{9}$$

where P_{01} denotes the probability that zero electrons are emitted in the first (ion impact) event and the correction terms in the brackets account for the summed probability that the electron amplification cascade dies in one of the subsequent (electron-induced) events. If the detector is operated at maximum gain, the correction terms can be assumed to be small compared to unity, and therefore $D(E) \cong 1 - P_{01}$. Inserting Eq. (8), this yields

$$D(E) \cong 1 - \exp(-\gamma_1). \tag{10}$$

As long as $\gamma_1 \ll 1$, Eq. (10) reduces to the linear dependence already described by Eq. (6). For the detection of large clusters, however, this condition may not be fulfilled. On the other hand, the impact velocity of large clusters will become comparable to or even smaller than the straight line threshold ν_0. In order to evaluate the detection probability in this regime, we must therefore insert Eq. (7) into Eq. (10). In principle, this can be done for each detected cluster size at different impact energies, and the resulting dependence can be fitted to the set of measured data. In order to illustrate this, Fig. 9 shows the measured relative signal enhancement upon increase of the ion impact energy from 3.7 to 6.2 keV as a function of the detected cluster size. Again, the solid and open symbols refer to analog detection and pulse counting, respectively. The solid line depicts a least-squares fit of the detection probability enhancement evaluated as described above to the pulse counting data in a cluster size range $10 \leqslant n \leqslant 30$. It is seen that up to $n = 30$ the measured data can be nicely approximated by a combination of Eqs. (7) and (10) using one set of parameters $a = 3.1 \times 10^{-2}$ s/km, $\nu_0 = 23.1$ km/s, and $\kappa = 4.6$. These values compare well with those obtained by Gilmore and Seah[32] from a fit of Eq. (7) to various sets of experimental electron yield data. Their validity can be further examined by predicting the signal enhancement for analog detection as given by Eq. (6). The resulting curve as a function of cluster size is included as a dashed line in Fig. 9. Note that this curve is fully determined by the parameter set evaluated from the pulse counting data: i.e., no fit to the analog data has been performed. The excellent quantitative agreement with the measured signal enhancement therefore indicates that Eqs. (6)–(10) provide a consistent picture of the post-acceleration data.

We can therefore use the parameter set in order to calculate the detection probability for In atoms and In_n clusters as a function of the cluster size. The results, normalized to the value of In atoms, are presented in Fig. 10. First, it is seen that the detection probability of small clusters *increases* with increasing cluster size, the magnitude of the effect being more pronounced for analog detection than for pulse counting. This finding is consistent with the electron yield data of Hofer[30] who studied the electron emission due to impact of vanadium cluster ions. In principle, such an increase is expected from Eq. (7) in the limit of large impact velocity, where the term in brackets approaches unity and therefore $\gamma_1 \propto n^{0.5}$. In the low-velocity limit, on the other hand, the asymptotic behavior of Eq. (7) leads to $\gamma_1 \propto n^{1-(\kappa+1)/2}$, and large clusters are thus discriminated as $n^{-1.8}$. The magnitude of this discrimination reaches about a factor of 30 at $n = 100$.

It should be noted at this point that for clusters containing more than 30 atoms deviations from the fit are observed in Fig. 9. Interestingly, the experimentally observed signal enhancement upon transition from 3.7 to 6.2 keV impact energy seems to become independent of cluster size in the limit of large size. Although such a leveling off is in principle expected from the theory described above, the saturated en-

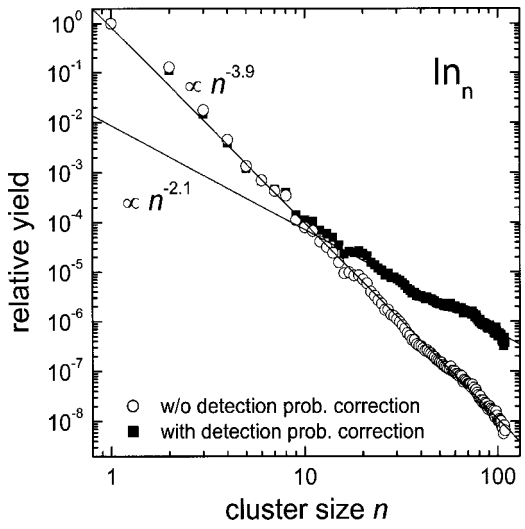

FIG. 11. Relative yields of In_n clusters sputtered from a pure, polycrystalline indium surface under bombardment with 15-keV Xe^+ ions. The data have been normalized to the partial yield of In atoms.

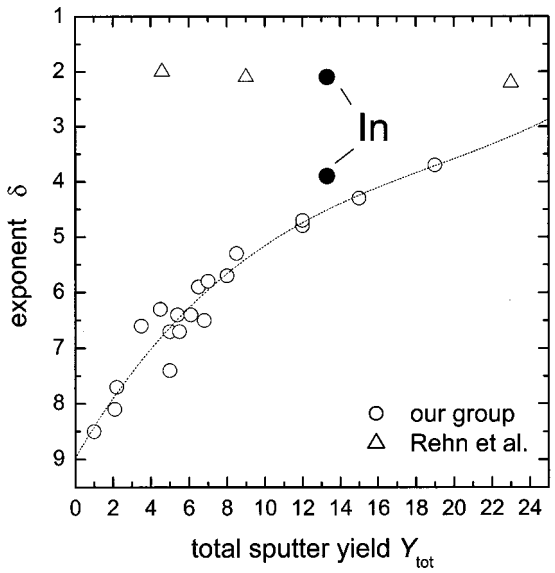

FIG. 12. Compilation of power-law exponents extracted from cluster yield distributions determined in our group vs total sputtering yield Y_{tot}. The In data (solid symbols) have been determined in this work: the remaining exponents (open symbols) corresponding to Ag, Cu, Al, Ge, Nb, and Ta are taken from previous publications. For comparison, the Au data of Rehn *et al.* (Ref. 23) have been included.

hancement would be predicted from the low-velocity asymptote of Eq. (7) to amount to a factor of

$$\left(\frac{E_2}{E_1}\right)^{(\kappa+1)/2} = 4.2, \tag{11}$$

instead of about 2.8 as observed, and should also be reached only at larger cluster sizes. Apart from the severe statistical scatter of the data, a possible cause of the deviation may be related to the assumption of a Poisson electron emission statistics in Eq. (8). From the experiments of Lakits *et al.*[33] it is known that this assumption may become worse with decreasing average electron yield. In fact, they demonstrated that the probability P_{01} may be underestimated at low average yields, thus leading to an overestimation of the detection probability in Eq. (10). It is not known how such an effect would modify the relative detection efficiency of different cluster sizes, and more data—particularly at much larger impact energies—are therefore certainly needed in order to clarify this point.

F. Cluster yields

With the corrections described above, it is now possible to convert the measured signals of sputtered neutral In atoms and In_n clusters into partial sputtering yields. Since the absolute value of the total sputtering yield has not been measured here, we present the relative yield distribution normalized to that of the atoms in Fig. 11. In order to put the results into context with available literature data, it should be stressed that none of the previously published experiments on sputtered clusters have been corrected for the cluster-size-dependent detection probability. Therefore, the data evaluated with all corrections except for detection probability are also included in the figure for comparison. It is immediately apparent that the detection probability plays an important role with respect to the interpretation of the data.

First, it is seen that the ''yield distribution'' evaluated without the detection probability correction can be very accurately approximated by a power-law decay according to

$$Y(n) = n^{-\delta}, \tag{12}$$

with an exponent $\delta = 3.9$. This finding is in good agreement with a number of mass spectrometric experiments on cluster yield distributions of mostly metal clusters sputtered from the respective clean metal surfaces that have been collected by several groups throughout the past decade.[7–10,13–15,18,34–36] In all cases, the resulting yield distributions could be well approximated by a power-law distribution with, however, largely varying exponents δ, the values of which were found to depend on the sputtering conditions employed. More specifically, it was established that the value of δ decreases if the sputtering conditions (i.e., the choice of target material, primary ion species, and kinetic energy) are varied such as to result in a higher total sputtering yield and vice versa. The apparent slope of our uncorrected data fits well into that picture. This is seen best in a compilation of exponents δ that have been determined in our group plotted against the total sputtering yield as shown in Fig. 12. Unfortunately, the sputtering yield of indium under bombardment with Xe^+ ions has not been measured experimentally and was therefore calculated using the SRIM2002 program package.[37]

The picture changes drastically if the correction for the cluster-size-dependent detection probability according to the data presented in Fig. 10 is invoked. Now, two different size regimes can be identified in which the yield distribution can still be approximated by power laws with, however, largely different exponents. For cluster sizes below $n = 20$, the cor-

rection is small and the distribution is roughly the same as the uncorrected one. For larger clusters, however, the yields are underestimated by Eq. (12) using $\delta = 3.9$. Instead, a gradual change to a different power-law dependence with an exponent of $\delta = 2.1$ is observed. This finding is important with respect to the theoretical understanding of cluster formation in sputtering. Although the experimental results could in some cases be qualitatively reproduced by molecular dynamics (MD) computer simulations of the cluster sputtering process, a rigorous theoretical explanation of the observed power-law size distributions has never been found. The particular problem is the strong variation of the exponent δ, which cannot be accounted for in any theoretical model of cluster formation in sputtering published to date. In fact, there are only two published model descriptions of cluster formation in sputtering that predict power-law cluster size distributions. The first, put forward by Bitensky and Parilis,[21] treats the cluster emission process as the result of a shock wave which is initiated by the primary ion impact, expands inside the solid, and fractures the surface, thus resulting in fragmentation into gas phase clusters. In fact, indications of shock waves have been found in MD simulations of sputtering.[38] The resulting size distribution of ejected species is predicted to be a power law with a fixed decay exponent around $\delta = 2$. The second model published by Urbassek[22] describes the cluster emission process as a thermodynamic expansion of the near-surface irradiated volume through the liquid-gas coexistence regime. Also in this model, a power-law size distribution is predicted with a fixed exponent $\delta = 7/3$. In both pictures, the sputtering conditions do not enter the exponent other than that they have to be chosen such as to warrant the validity of the model.

The data depicted in Fig. 11 now present the first indication that the observation of a unique power-law distribution over the whole cluster size range that has been characteristic of previous mass spectrometric experiments may be restricted to small- and medium-sized clusters only. In fact, the data suggest that different size ranges of sputtered clusters must be described by different model descriptions. In the limit of large cluster size, collective atomic motion dominates and both the shock-wave or thermodynamic models describe the measured cluster yields. This finding is in excellent agreement with the results of a recent experiment performed by Rehn *et al.*,[23] who studied the emission of very large clusters ($n > 500$) in a transmission sputtering experiment by bombarding a thin gold foil with high energy (400–500 keV) rare gas ions. In their setup, the sputtered clusters were collected on a graphite foil and identified using a high-resolution transmission electron microscopy, thereby avoiding the detection efficiency problem of mass spectrometric experiments. It was found that the observed cluster size distribution could in all cases be nicely approximated by a power-law distribution with $\delta \sim 2$, regardless of the total sputtering yield.

In principle, it would be of interest to determine whether the shock wave or the thermodynamical model provides a better description of the measured data. On the basis of the numeric value of the decay exponents determined here and in Ref. 23, it is not possible to discern between both models. Apart from the uncertainty of the experimental exponents (± 0.1), this is primarily related to the fact that two different exponents (5/3 or 7/3) are given in Ref. 21, which, as explicitly stated by the authors, are moreover only approximate. In principle, MD simulations can be invoked in order to distinguish between both mechanisms. Unfortunately, the range of cluster sizes tractable by such simulations is limited by the statistics of the calculation, and the yield distribution of clusters containing more than about ten atoms therefore cannot be directly predicted. The simulations reveal, however, an interesting aspect related to the time scale on which the formation and emission of larger clusters proceeds. On the average, it is consistently found that larger clusters are formed at later stages of the collision cascade initiated by the projectile impact,[39–41] the emission of the largest clusters being observed at several picoseconds or even longer after the projectile impact. At least for the case of backward sputtering, this observation points towards a thermodynamical description, since a shock wave generated at a depth of several angstroms should propagate to the surface on a faster time scale. Anyway, it is apparent that the emission of large clusters must be governed by different mechanisms than the fast collisional processes leading to the ejection of small particles.

On the other end of the observable size range, the mass spectrometric yield distributions of very small clusters containing only a few atoms can often be approximated by exponential size distributions.[4,5,15,42] Distributions of this kind are predicted by statistical models that treat the cluster emission as a more or less uncorrelated ejection of the constituent atoms.[1] Since the statistical probability for independent ejection of many atoms into essentially the same phase space interval becomes exceedingly small, it is apparent that clusters containing more than a few atoms cannot be formed in such a way. The formation of medium-sized species must therefore already be the result of collective atomic motion at or below the surface. The underlying mechanisms—though difficult to describe in an analytic model—can be investigated by MD simulations. Such calculations reveal that the formation of medium-sized clusters is coupled to the occurrence of large, rare events where many atoms are set in motion and ejected.[39,40,43] The probability of such events, on the other hand, is connected with the average number of sputtered atoms and increases with increasing total sputtering yield. In fact, the MD simulations predict nascent cluster yield distributions which closely follow a power-law distribution with exponents varying as a function of the sputtering conditions in a similar manner as those observed experimentally.[41] It should be noted, however, that the nascent clusters identified immediately above the surface are highly vibrationally excited and therefore decompose by unimolecular fragmentation processes on their flight away from the surface.[44] In fact, a constant internal energy of the order of 1 eV/atom is frequently found in the simulations[41] and could also be verified experimentally.[45,46] Since most experimental detection schemes are sensitive to the metastable (''final'') products of such fragmentation reactions, the weight of the observed size distribution is pushed towards smaller fragments, an effect which acts to increase the mea-

sured power law exponent. The correlation with the sputtering conditions remains, however, unchanged.

IV. CONCLUSION

The present experiment extends the observable size range of neutral clusters that are generated by sputtering beyond a cluster size of 200 atoms. In order to investigate the distribution of partial sputter yields as an important quantity characterizing the cluster formation process, the mass spectrometric signals of different clusters are corrected for postionization efficiency, charge-state distribution, velocity distribution, and cluster-size-dependent detection probability. The results demonstrate that for clusters containing more than about 20 atoms the detection probability becomes an exceedingly important parameter that needs to be characterized in order to arrive at a quantitative determination of the true cluster size distribution. While the uncorrected data exhibit the simple inverse power-law size distribution that has already been observed in previous experiments on other metallic systems, the corrected distribution reveals a separation into different size regimes. For clusters containing less than about 20 atoms, the yield distribution is found to decay with increasing cluster size according to an inverse power law with an exponent of -3.9. For clusters composed of more than 20 atoms, on the other hand, the yield distribution changes towards a different power law with a decay exponent of -2.1, a behavior which is in good agreement with electron microscopic results on the yield distributions of very large clusters containing more than 500 atoms.

It is apparent that the present work closes the gap between the different types of experimental data on cluster formation in sputtering that have been collected in mass spectrometric experiments on the one hand and electron microscopic investigations on the other. From the results, a consistent picture with respect to the size distribution of sputtered metallic clusters emerges. For *small* clusters in the size range up to several ten atoms, the measured yield distribution is characterized by a power-law exponent which largely depends on the sputtering conditions. This behavior is also reproduced in computer simulations of the cluster sputtering process, a comprehensive theoretical approach explaining the power law in this size range and, in particular, the dependence of the decay exponent on the sputtering conditions is, however, still lacking. Large clusters, on the other hand, are characterized by a weaker size distribution, which agrees well with that predicted by hydrodynamical or thermodynamical models of cluster formation. In accordance with similar indications from MD simulations, these species must therefore be formed in a very late stage of the collision cascade initiated by the impinging projectile, where the energy has been sufficiently redistributed to permit a local thermodynamic description of particle motion inside the volume from which the desorbed particles originate.

ACKNOWLEDGMENT

One of the authors (C.S.) would like to thank the University of Essen for financial support.

[1] H. M. Urbassek and W. O. Hofer, Mat. Fys. Medd. K. Dan. Vidensk. Selsk. **43**, 97 (1993).
[2] I. Katakuse, T. Ichihara, Y. Fujita, T. Matsuo, T. Sakurai, and H. Matsuda, Int. J. Mass Spectrom. Ion Processes **74**, 33 (1986).
[3] R. Heinrich, C. Staudt, M. Wahl, and A. Wucher, in *Secondary Ion Mass Spectrometry (SIMS XII)*, edited by A. Benninghoven, P. Bertrand, H. N. Migeon, and H. W. Werner (Elsevier Science, Amsterdam, 2000), p. 111.
[4] H. Gnaser and W. O. Hofer, Appl. Phys. A: Solids Surf. **48**, 261 (1989).
[5] A. Wucher and M. Wahl, in *Secondary Ion Mass Spectrometry (SIMS X)*, edited by A. Benninghoven, B. Hagenhoff, and H. W. Werner (Wiley, Chichester, 1997), p. 64.
[6] M. Wahl and A. Wucher, Nucl. Instrum. Methods Phys. Res. B **94**, 36 (1994).
[7] S. R. Coon, W. F. Calaway, J. W. Burnett, M. J. Pellin, D. M. Gruen, D. R. Spiegel, and J. M. White, Surf. Sci. **259**, 275 (1991).
[8] S. R. Coon, W. F. Calaway, M. J. Pellin, and J. M. White, Surf. Sci. **298**, 161 (1993).
[9] Z. Ma, S. R. Coon, W. F. Calaway, M. J. Pellin, D. M. Gruen, and E. I. Nagy-Felsobuki, J. Vac. Sci. Technol. A **12**, 2425 (1994).
[10] S. R. Coon, W. F. Calaway, and M. J. Pellin, Nucl. Instrum. Methods Phys. Res. B **90**, 518 (1994).
[11] C. S. Hansen, W. F. Calaway, B. V. King, and M. J. Pellin, Surf. Sci. **398**, 211 (1998).
[12] T. J. Colla, H. M. Urbassek, A. Wucher, C. Staudt, R. Heinrich, B. J. Garrison, C. Dandachi, and G. Betz, Nucl. Instrum. Methods Phys. Res. B **143**, 284 (1998).
[13] R. Heinrich and A. Wucher, Nucl. Instrum. Methods Phys. Res. B **140**, 27 (1998).
[14] A. Wucher and M. Wahl, Nucl. Instrum. Methods Phys. Res. B **115**, 581 (1996).
[15] A. Wucher, M. Wahl, and H. Oechsner, Nucl. Instrum. Methods Phys. Res. B **83**, 73 (1993).
[16] A. Wucher, R. Heinrich, R. M. Braun, K. F. Willey, and N. Winograd, Rapid Commun. Mass Spectrom. **12**, 1241 (1998).
[17] R. Heinrich and A. Wucher, in *Secondary Ion Mass Spectrometry (SIMS XI)*, edited by G. Gillen, R. Lareau, J. Bennett, and F. Stevie (Wiley, Chichester, 1998), p. 949.
[18] C. Staudt and A. Wucher, in *Resonance Ionization Spectroscopy*, edited by J. C. Vickerman and E. K. Parks (AIP, Woodbury, NY, 1998), p. 217.
[19] C. Staudt, R. Heinrich, and A. Wucher, Nucl. Instrum. Methods Phys. Res. B **164–165**, 677 (2000).
[20] A. Wucher, M. Wahl, and H. Oechsner, Nucl. Instrum. Methods Phys. Res. B **82**, 337 (1993).
[21] I. S. Bitensky and E. S. Parilis, Nucl. Instrum. Methods Phys. Res. B **21**, 26 (1987).
[22] H. M. Urbassek, Nucl. Instrum. Methods Phys. Res. B **31**, 541 (1988).

[23] L. E. Rehn, R. C. Birtcher, S. E. Donnelly, P. M. Baldo, and H. Furutani, Phys. Rev. Lett. **87**, 207601 (2001).
[24] A. Wucher, R. Heinrich, and C. Staudt, in *Secondary Ion Mass Spectrometry (SIMS XII)*, edited by A. Benninghoven, P. Bertrand, H. N. Migeon, and H. W. Werner (Elsevier Science, Amsterdam, 2000), p. 143.
[25] I. Katakuse, T. Ichihara, Y. Fujita, T. Matsuo, T. Sakurai, and H. Matsuda, Int. J. Mass Spectrom. Ion Processes **67**, 229 (1985).
[26] Y. Saito, I. Katakuse, and H. Ito, Chem. Phys. Lett. **161**, 332 (1989).
[27] M. Pellarin, B. Baguenard, C. Bordas, M. Broyer, J. Lerme, and J. L. Vialle, Z. Phys. D: At., Mol. Clusters **26**, 137 (1993).
[28] Z. Ma, W. F. Calaway, M. J. Pellin, and E. I. Nagy-Felsobuki, Nucl. Instrum. Methods Phys. Res. B **94**, 197 (1994).
[29] M. W. Thompson, Philos. Mag. **18**, 377 (1968).
[30] W. O. Hofer, Scanning Microsc. Suppl. **4**, 265 (1990).
[31] M. P. Seah, J. Electron Spectrosc. Relat. Phenom. **50**, 137 (1990).
[32] I. S. Gilmore and M. P. Seah, Int. J. Mass Spectrom. Ion Processes **202**, 217 (2000).
[33] G. Lakits, F. Aumayr, and H. Winter, Rev. Sci. Instrum. **60**, 3151 (1989).
[34] C. E. Young, W. F. Calaway, M. J. Pellin, and D. M. Gruen, J. Vac. Sci. Technol. A **2**, 693 (1984).
[35] R. Heinrich and A. Wucher, Nucl. Instrum. Methods Phys. Res. B **164–165**, 720 (2000).
[36] R. Heinrich and A. Wucher, Nucl. Instrum. Methods Phys. Res. B **193**, 781 (2002).
[37] See http://www.srim.org
[38] K. T. Waldeer and H. M. Urbassek, Nucl. Instrum. Methods Phys. Res. B **73**, 14 (1993).
[39] G. Betz and W. Husinsky, Nucl. Instrum. Methods Phys. Res. B **102**, 281 (1995).
[40] T. J. Colla and H. M. Urbassek, Nucl. Instrum. Methods Phys. Res. B **164–165**, 687 (2000).
[41] A. Wucher and B. J. Garrison, J. Chem. Phys. **105**, 5999 (1996).
[42] W. Gerhard and H. Oechsner, Z. Phys. B **22**, 41 (1975).
[43] M. Lindenblatt, R. Heinrich, A. Wucher, and B. J. Garrison, J. Chem. Phys. **115**, 8643 (2001).
[44] A. Wucher and B. J. Garrison, Phys. Rev. B **46**, 4855 (1992).
[45] A. Wucher, A. D. Bekkerman, N. Kh. Dzhemilev, S. V. Verkhoturov, and I. V. Veryovkin, Nucl. Instrum. Methods Phys. Res. B **140**, 311 (1998).
[46] A. Wucher, N. Kh. Dzhemilev, I. V. Veryovkin, and S. V. Verkhoturov, Nucl. Instrum. Methods Phys. Res. B **149**, 285 (1999).